Clusterization and Strong Coupled Channels Effects in Reactions of Deuteron Interaction with ^{9}Be Nuclei

B A Urazbekov[1,2,3]**, A S Denikin**[2,3]**, S M Lukyanov**[3]**,
N Itaco**[1]**, D M Janseitov**[3,4]**, K Mendibayev**[3,5,6]**, V Burjan**[7]**,
V Kroha**[7]**, J Mrazek**[7]**, W H Trzaska**[8]**, M N Harakeh**[9]**,
D Etasse**[10]**, I Stefan**[11]**, D Verney**[11]**, T Issatayev**[3,5]**,
Yu E Penionzhkevich**[3]**, K A Kuterbekov**[5]** and
T Zholdybayev**[6]

[1] Dipartimento di Matematica e Fisica, Università degli Studi della Campania
Luigi Vanvitelli, I-8110 Caserta, Italy
[2] Dubna State University, 141982 Dubna, Russia
[3] Joint Institute for nuclear research, 141980 Dubna, Russia
[4] Al-Farabi Kazakh National University, 050040 Almaty, Kazakhstan
[5] L N Gumilyov Eurasian National University, 010008 Astana, Kazakhstan
[6] Institute of Nuclear Physics, 050032 Almaty, Kazakhstan
[7] Nuclear Physics Institute CAS, 25068 Řež, Czech Republic
[8] Department of Physics, University of Jyväskylä, FIN-40014 Jyväskylä, Finland
[9] KVI-CART, University of Groningen, 9747 AA Groningen, The Netherlands
[10] Normandie Université, ENSICAEN, UNICAEN, CNRS/IN2P3, LPC Caen,
14000 Caen, France
[11] Institut de Physique Nucléaire, Univ. Paris-Sud, Université Paris-Saclay,
F-91406 Orsay, France

E-mail: `bakytzhan.urazbekov@gmail.com`

Abstract. Angular distributions of protons, deuterons, tritons and alpha particles emitted in the d + ^{9}Be reaction at E_{lab}=19.5 and 35.0 MeV are measured. The elastic channel is analysed in the framework of both the Optical Model and the Coupled Channel approach. The interaction potential of the d + ^{9}Be system is calculated in the framework of the Double Folding model using the $\alpha + \alpha + n$ three body wave function of the ^{9}Be nucleus. The deformation parameter β_2 is obtained for the transition $\frac{3}{2}^- \rightarrow \frac{5}{2}^-$ in ^{9}Be. The (d,p) and (d,t) one nucleon exchange reactions are analysed within the coupled reaction channel approach. The spectroscopic amplitudes for the different nuclear cluster configurations are calculated. Differential cross sections for the reaction channel ^{9}Be(d,α)^{7}Li are calculated including all possible reaction mechanisms within the coupled reaction channel method as well. Corresponding contributions to the cross sections are analysed.

Keywords: cluster structure, optical model, CRC, DWBA, spectroscopic amplitudes, double folding, elastic and inelastic scattering, few-nucleon transfer reactions

1. Introduction

The cluster structure of nuclei arises from a correlated motion of nucleons inside a nucleus. In this regime a simple subgroup can be seen as a single particle. This kind of behaviour can give insights into numerous characteristics of the nucleus, as well as affect the processes of nuclear reactions. Investigation of the cluster structure in nuclei is still one of the priority problems of modern nuclear physics in connection with the intensive developments of experimental devices.

There is a row of stable nuclei exhibiting the cluster structure, but ^{9}Be is particularly worthy of attention due to the following reasons:

- stable nucleus with the low binding energies of neutron S_n=1.665 MeV, and α-particle S_α=2.462 MeV [1];
- the deformed shape reflected in the nuclear quadrupole moment, Q= +52.9 mb [2];
- the Borromean structure of the ground state;

These aspects led to take ^{9}Be as a subject for fundamental as well as applied researches studies.

Regarding nuclear technologies, ^{9}Be is a good wall material in thermonuclear devices [3, 4]. For instance, for fusion device types a value of some dozens of percent of soft wall material is expected in the case of ^{9}Be [4]. The nucleus has been chosen as it represents the best compromise based on its ability to be well split into two energetic α-particles by the use of γ and e^-, which are efficient promoters of thermonuclear burning. Since they can be confined by electromagnetic fields and their energy affects the temperature of the burning zone.

Scattering of the simplest projectile, such as ^{1,2}H or ^{3,4}He, on a target is a standard tool for fundamental study the structure of nuclei. This method involves measuring the angular distribution of the nuclear reaction products. It is well known that the energy and angular distributions of projectile-like particles give information about internal structure of target-like nuclei.

In our previous works [5, 6, 7] the ^{3}He interaction with ^{9}Be was studied and angular distributions of the reaction products in the following exit channels: ^{3}He+^{9}Be, ^{5}He+^{7}Be, ^{5}Li+^{7}Li, ^{6}Be+^{6}He, and ^{6}Li+^{6}Li, were measured. The obtained data were analysed within the framework of the Optical Model (OM), the Coupled Channel (CC) and the distorted wave Born approximation (DWBA) approaches. The performed analysis of the experimental data showed sensitivity of cross section on the potential parameters in the exit channels. Moreover, these experiments were designed to study the breakup reactions with ^{9}Be in attempt to determine contributions of the channels through the ^{8}Be+n and ^{5}He+α structure within the inclusive measurements. It was found that the ratio 2.7 ÷ 1 could be assigned to the contributions of these two channels respectively. The determined value justifies that the ^{5}He+α breakup channel plays an important role as well.

Basing on the Borromean structure of ^{9}Be, special attention was focused on the breakup processes resulting in the ^{9}Be(^{6}Li, ^{6}Li)^{9}Be* nuclear reaction [8, 9]. The excited nucleus ^{9}Be* can decay either directly into the $\alpha+\alpha+n$ three-body system or through one of the unstable nuclei, such as ^{5}He and ^{8}Be. Thereby, these relatively recent experimental studies explicitly confirm the cluster structure of ^{9}Be. The calculated branching ratios show that the low lying excited states, at $E_x < 4.0$ MeV, are mostly populated with the ^{8}Be+n configuration. In other condition, the ^{5}He+α configuration plays a significant role.

Another aspect of finding the cluster structure is its attandance in the nuclear reaction mechanisms. Indeed, since the papers of Detraz *et al* [10, 11], the multiparticle-multihole structures have been expected at rather low excitation energies in nuclei. In this case, it can be understood that the nucleons are transferred as a whole strongly correlated cluster, which has the internal quantum numbers of a free particle.

The interaction of deuteron and alpha particles with ^{9}Be was studied with regard to the cluster structure [12, 13]. The interaction potential of colliding nuclei was built within the framework of the Double Folding model using the three body wave function. Approbation of the double folded potential was carried out within the OM, DWBA at laboratory energies 10-30 MeV/nucleon. Comparison of theoretical cross sections with experimental data led to the applicability of the double folding potential based on the three body wave function.

The current work devouted to the investigation of the cluster structure of the ^{9}Be nucleus studing the nuclear reactions caused by a deuteron beam at 19 MeV and 35 MeV energies. In the exit channel the simplest particles, such as p, d, t, and α-particles, were registered and their angular distributions were obtained. A comparative analysis of experimental data
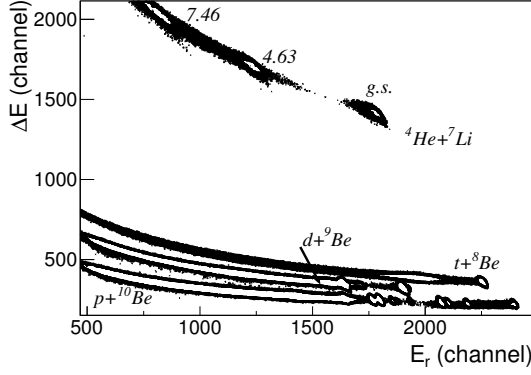
Figure 1. Particle identification plots for the products of the ^{2}H+^{9}Be reaction: p, d, t, and ^{4}He. ΔE is the energy loss and E_r is the residual energy. Excited states for the ^{7}Li reaction channel ^{7}Li+α are indicated.

and theoretical calculations has been performed.

2. Experimental Method

The experiment has been performed at the INP (Řež, Czech Republic) and in the Physics Department of Jyväskylä University (Jyväskylä, Finland). The beam energy of ^{2}H ions produced from the cyclotrons were at energies 19.5 and 35 MeV. The average beam current during the experiment was maintained at 20 nA. The self-supporting ^{9}Be target was prepared from a thin beryllium foil with the 99 % purity. A set of four telescopes was used with the purpose of registering the simplest particle of output channels. Each telescope was contained the ΔE_0, ΔE, E_r detectors with the respective thickness of 12 μm, 100 μm and 3 mm. To detect reaction product in narrow divergence, telescopes were mounted at a distance of $\sim$25 cm from the target. Each telescope was shielded by a Cu-Pb collimator with thickness of 3 mm and hole with diameter of 3 mm. The telescopes were mounted on rotating supports, which allow us to obtain data from $\theta_{lab} = 20°$ to $107°$ in steps of $1-2°$.

The particles were identified based on the energy-loss measurements of ΔE and the residual energy E_r, i.e., by the so-called ΔE-E method. An example of two-dimensional plots (yield vs. energy loss ΔE and residual energy E_r) is shown in Fig. 1.

The capability of current experimental technique is in identification of the particles p, d, t, and α and in the determination of their total deposited energies. The spectra of total deposited energy are shown in Fig. 2. All the peaks from Fig. 2 has been identified and assigned to the ground and the excited states of the ^{10}Be, ^{9}Be, ^{8}Be, ^{7}Li nuclei as the complementary products for the detected particles
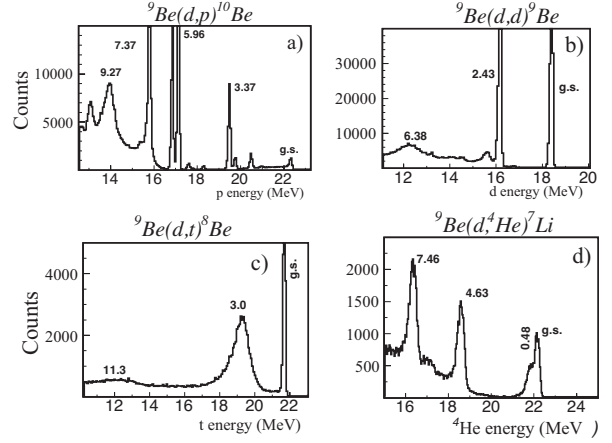
Figure 2. Total deposited energy spectra measured at θ_{lab}=32° for the detected p (panel a), d (panel b), t(panel c), and α(panel d). The ground and the excited states of ^{7}Li for the detected complementary product α as well as the ground states and the excited states for ^{8}Be, ^{9}Be, and ^{10}Be in the case of detected t, d, and p, as complementary products, respectively, are unambiguously identified.

p, d, t, α, respectively.

3. Data Analysis and Results

3.1. Elastic scattering

The theoretical calculations of the deuteron elastic scattering on ^{9}Be at 19.5 and 35 MeV energies have been made in the framework of the OM. The model suggests interaction between two colliding nuclei in the following way:

$$U(R) = -V^V(R) - iW^V(R) + V^{SO}(R)(\mathbf{l} \cdot \sigma) + V^C(R), \tag{1}$$

where V^V, W^V, V^{SO}, and V^C are real volume, imaginary volume, spin-orbit and Coulomb potential, respectively. In this work the real part of the optical potential were obtained by means of the Double Folding model

$$V^V(R) = N_R V^{DF}(R) \tag{2}$$

with normalization factor N_R. For convenience in the OM and CC (CRC) calculations the potential can be fitted by means of the sum of three Woods-Saxon potentials:

$$V^V(R) = \sum_{i=1}^{3} V^i f^{R_i, a_i}(R), \tag{3}$$

$$f^{R_V, a_V}(R) = \frac{1}{1 + exp\frac{R - R_V}{a_V}}. \tag{4}$$

The DF potential was calculated using the effective M3Y-Paris nucleon-nucleon potential and the nuclear-matter-densities of projectile and target nuclei.
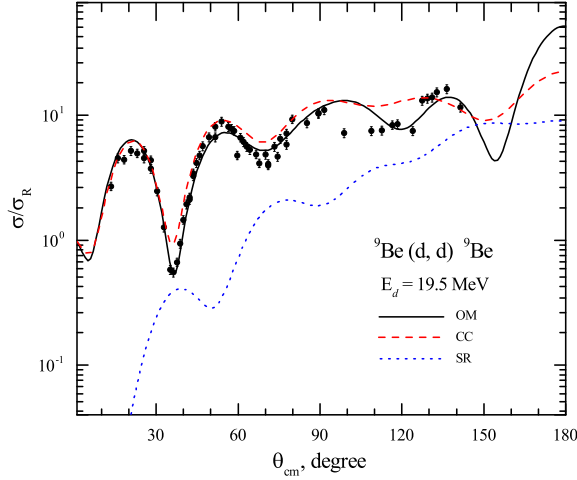
Figure 3. The angular distribution of elastic scattering data of d from ^{9}Be at laboratory energy 19.5 MeV in comparison with theoretical calculations within the OM (solid curve) and CC (dashed curve) method with spin reorientation (dotted curve).

Figure 4. The same as caption in Fig. 3 at laboratory energy 35 MeV.

In order to calculate the ^{9}Be matter distribution we applied the $\alpha + \alpha + n$ three body model (for more details, see Ref. [12]), while the matter density distribution of the deuteron projectile was chosen in form

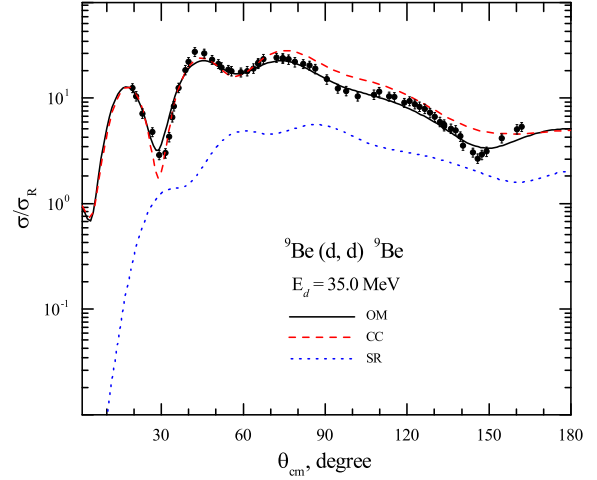$$\rho\left(\frac{1}{2}r\right) = \int |\Psi(\mathbf{r})| d\Omega_r. \tag{5}$$

Spin-orbit term has standard form

$$V^{SO}(R) = V_0^{SO}\left(\frac{\hbar}{m_\pi c}\right)^2 \frac{1}{R}\frac{d}{dR}f^{R_{SO}a_{SO}}(R). \tag{6}$$

The Coulomb term has been taken as the interaction of a point-charge with a uniformly charged sphere

$$V^C(R) = \begin{cases} \dfrac{Z_1 Z_2 e^2}{2R_C}\left(3 - \dfrac{R^2}{R_C^2}\right), & \text{for R} \leq R_C, \\ \dfrac{Z_1 Z_2 e^2}{R}, & \text{for R} > R_C. \end{cases} \tag{7}$$

The parameters of the imaginary part of the optical potential was obtained by fitting the theoretical cross sections to the experimental data at 19.5 MeV

and 35 MeV energies. As a starting point the same parametrizations of the real part were used. The obtained potential parameters after fitting are listed in Table 1 for both 19.5 MeV and 35.0 MeV energies.

The comparison of the results of theoretical calculations with the measured data on the elastic scattering at 19.5 MeV and 35.0 MeV energies are plotted in Figures 3 and 4 correspondingly. The cross sections obtained in the framework of the OM with the DF potential are shown as the solid curve. Theoretical results taken by means of the OM gives an excellent agreement, $\chi^2 \approx 2.5$, with experimental data. The parameters of parametrised double folding potential are presented in Tab. 1.
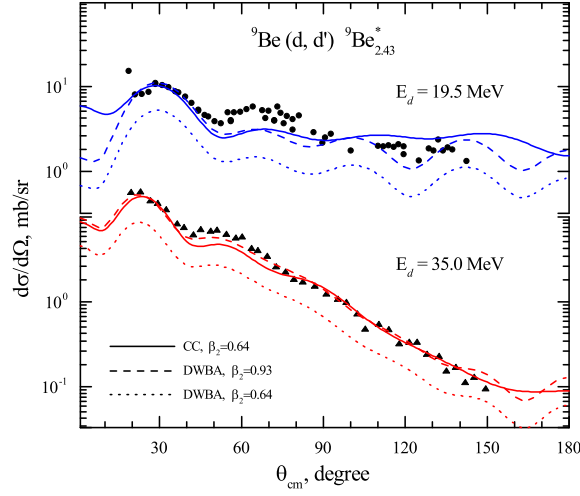
The elastic scattering cross sections were also analysed within the CC approach (for more details, see the next section). We coupled the $5/2^-$ and $7/2^-$ rotational bands of ^{9}Be with the ground state. Also the spin reorientations were included to the coupling. The calculation results within the CC method are represented as dashed curve in Figures 3 and 4 for both energies. Analysis shows a valuable contribution of the

Table 1. Parametrised double folding potentials of the d+^{9}Be system used in the OM, the CC and the DWBA calculations.

E_d, MeV	i	V_0, MeV	r_v^a, fm	a_v, fm	W_0, MeV	r_w^a, fm	a_w, fm	V_0^{SO}, MeV	N_R,	r_C^a, fm	χ^2
19.5	1	6.18	0.328	0.308	3.99	0.328	0.127	3.275	1.22	0.809	2.490
	2	70.97	0.746	0.831	25.50 (17.5^b)	0.746	0.766				
	3	0.605	1.491	1.724	0.924	1.491	2.238				
35.0	1	5.941	0.328	0.308	7.07	0.612	0.108	3.275	1.17	0.809	2.503
	2	68.68	0.746	0.831	22.50 (17.5^b)	0.838	0.731				
	3	0.58	1.491	1.724	0.999	1.377	1.856				

^{a} Radii are defined as $R_i = r_i\left(A_P^{1/3} + A_T^{1/3}\right)$.

^{b} The values are used in CRC calculations.

Figure 5. The cross sections of inelastic scattering ^{9}Be(d,d)^{9}Be* (E_{exc}=2.43 MeV) at laboratory energies 19.5 MeV (full circle) and 35 MeV (full triangle). Theoretical curves are described in the text.

spin reorientation (dotted curve) of the ground state of ^{9}Be. Especially it is manifested at back scattering angles. It should be noted that such kind of behaviour of spin reorientation effect also was mentioned in Ref. [14]. Contributions of the $5/2^-$ and $7/2^-$ rotational bands to the ground state were not noticed in the analysis. The CC calculation results are in good agreement with the experimental data. An explicit implementation of the inelastic channel led to change the absolute value of the W_0 parameters. The changes are presented in Tab. 1.

3.2. Inelastic scattering

The CC and the DWBA approaches have been applied to analyse the measured inelastic scattering data corresponding to the ^{9}Be($5/2^-$, 2.43 MeV) excitation. Calculations were performed employing the FRESCO code [15] and the DWUCK5 code [16] which are available in the NRV knowledge-base [17].

In order to describe measured experimental data one consider the ^{9}Be target having the quadrupole deformation. Thus the ^{9}Be spectrum consists the rotational band including the ground state, $5/2^-$ state at 2.43 MeV and $7/2^-$ state at 6.38 MeV. Coupling to these states were taken into account within the couple channel approach. The spin reorientations were also taken into account. The coupling interaction has the usual form:

$$V_\lambda(R) = -\beta_\lambda R_V \left| \frac{dV^V}{dR} \right| - i\beta_\lambda R_W \left| \frac{dW^D}{dR} \right|, \qquad (8)$$

where β_λ is the deformation parameter of λ multipole describing the target-nucleus form. Here we as usual neglect the contribution of the Coulomb interaction.

The calculated cross sections for inelastic scattering are shown in Fig. 5. The solid curves correspond to the results obtained within the CC approach, while the dashed and dotted curves were obtained within the DWBA approach using different values of the deformation parameter β_2. Used potential parameters are listed in Table 1.

All the results in Fig. 5 are in good agreement with experimental data. The quadrupole deformation parameter $\beta_2 = 0.64$ extracted within couple channel model is in consistence with the previous studies [5, 18].

In the case of DWBA calculations one use the DF potential (see Table 1) for both the entrance and the exit channels. The DWBA angular distributions very well reproduce the structure of experimental data but distinctly underestimate them when the deformation parameter $\beta_2 = 0.64$ is used (see the dotted curves in Fig. 5). In order to get the best fit the deformation parameter must be increased up to $\beta_2 = 0.93$ which is quite close to the values reported in previous studies (see, for example, [19, 20]).

Thus one may confirm that channel coupling and the effects of spin reorientation enhance the cross section that results in the reduction of the deformation parameter. However, the DWBA approach takes into account only first order contributions to the transition amplitude. In particular, it also describes only general features of the angular distributions and overestimates the deformation parameter in order to compensate the difference between the experimental data and the DWBA cross sections.

3.3. One nucleon transfer reactions

The one neutron pick-up ^{9}Be(d,t)^{8}Be and stripping ^{9}Be(d,p)^{10}Be reactions were analyzed here within the
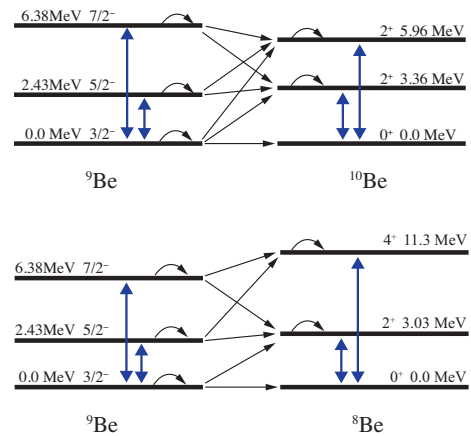
Figure 6. The target coupling schemes in the ^{9}Be(d,p)^{10}Be (upper) and the ^{9}Be(d,t)^{8}Be (lower) nuclear reactions. The bold two headed arrows indicate Eλ transitions. The spin reorientation effects are indicated as back pointing arrows.
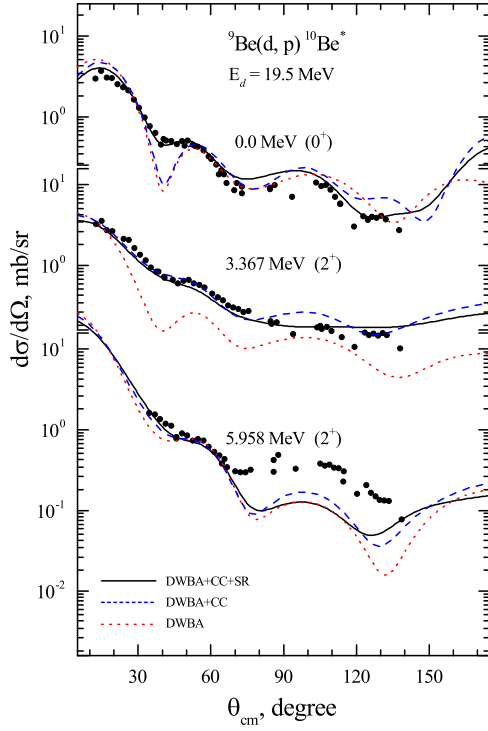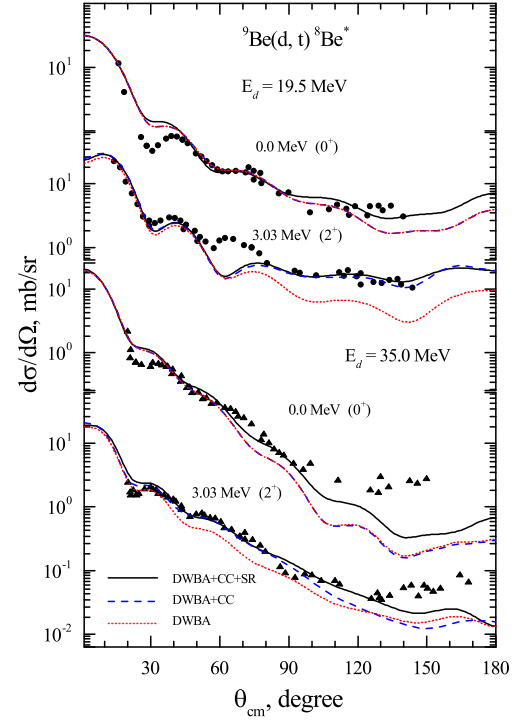
Figure 7. Differential cross sections for the ^{9}Be(d,p)^{10}Be* reactions at 19.5 MeV for the neutron transferred to the different final states (indicated near the curves) of the ^{10}Be product. The experimental data are shown in comparison with theoretical results obtained within the CRC method.

Figure 8. Differential cross sections for the ^{9}Be(d,t)^{8}Be* reactions at 19.5 and 35 MeV corresponding to the ^{8}Be product in the different final states (indicated near the curves) in the exit channel. The experimental data are shown in comparison with theoretical results obtained within the CRC method.

framework of the Coupled Reaction Channels (CRC).

The double folding potential given in Table 1 were used in the CRC calculations for the entrance channel as well as the global optical parametrizations from Ref. [21, 22] were used for the exit channels. The coupling schemes of target nuclei for the ^{9}Be(d,p)^{10}Be and ^{9}Be(d,t)^{8}Be reactions are illustrated in Fig. 6. The states of ^{10}Be, 2^+_1 and 2^+_2, as well as the low-lying excited states of ^{8}Be, 2^+ and 4^+, were implemented to the coupling scheme. Also, the schemes take into account the spin reorientations of states on the condition $J \neq 0$.

In order to construct the bound state wave functions of the transferred particle in entrance and exit channels one employed the common method, i.e. fitting the depth of the corresponding Woods-Saxon potential to the known binding energy. The reduced radius and diffuseness in this case are set to be equal $r = 1.25$ fm and $a = 0.65$ fm correspondingly. If the transfer takes place to the final unbound states, the depth of the potential for this state was adjusted to provide the binding energy equal to -0.1 MeV in accordance with the recommendation given in Ref. [18].

The spectroscopic amplitude $\mathcal{S}$ for an addition of particle from a Core J_{core} to a Composite J_{com}

is related to the matrix element of the creation operator $\hat{a}^\dagger$:

$$\mathcal{S}_{NL_J} = \frac{\langle J_{com} \| \hat{a}^\dagger_{NL_J} \| J_{core} \rangle}{\sqrt{2J_{com}+1}} \tag{9}$$

where NL_J is the set of particle quantum numbers. The spectroscopic amplitudes for one particle states were calculated by means of the $ANTOINE$ code [23] using the effective Cohen-Kurath interaction for p-shell nuclei [24]. The calculated spectroscopic amplitudes for the one nucleon transfer reactions are listed in Tab. 2.

Angular distributions of the ^{9}Be(d,p)^{10}Be nuclear reaction at E_d=19.5 MeV are shown in comparison with the theoretical curves made in the framework of the CRC mothod in the Fig. 7.

In order to study the couplings of the input channels, the outputs were fixed using deformation parameter of ^{8}Be from Ref. [27], for ^{10}Be from Ref. [18]. The direct transitions from ground state is indicated by the dotted line (DWBA). The contributions of the transitions from excited states (CC), spin reorientations (SR) are indicated by dashed and solid lines, respectively. During the analysis, it was found that spin reorientation has a significant contribution in the p + ^{10}Be^{gs} channel, especially in

Table 2. Spectroscopic amplitudes used in CRC calculations for the Composite = Core + Cluster system. The one nucleon spectroscopic amplitudes calculated by means of the *ANTOINE* code [23]. The alpha spectroscopic amplitudes were taken from [25, 26].

| Composite	$2J_{com}$	Core	$2J_{core}$	Cluster	2J	SA	Composite	$2J_{com}$	Core	$2J_{core}$	Cluster	2J	SA
^{9}Be	3	^{8}Be	0	n	3	−0.761	^{9}Be	3	^{8}Li	2_1	p	1	−0.444
^{9}Be	3	^{8}Be	4	n	3	0.816	^{9}Be	3	^{8}Li	6	p	3	−0.592
^{9}Be	3	^{8}Be	4	n	1	−0.242	^{9}Be	3	^{8}Li	2_2	p	3	−0.236
^{9}Be	5	^{8}Be	4	n	3	0.986	^{9}Be	3	^{8}Li	2_2	p	1	0.036
^{9}Be	5	^{8}Be	4	n	1	−0.417	^{9}Be	5	^{8}Li	4	p	3	0.593
^{9}Be	5	^{8}Be	8	n	3	−0.374	^{9}Be	5	^{8}Li	4	p	1	0.515
^{9}Be	7	^{8}Be	4	n	3	−0.457	^{9}Be	5	^{8}Li	2_1	p	3	−0.672
^{9}Be	7	^{8}Be	8	n	3	0.919	^{9}Be	5	^{8}Li	6	p	3	−0.571
^{9}Be	7	^{8}Be	8	n	1	−0.429	^{9}Be	5	^{8}Li	6	p	1	−0.171
^{8}Be	0	^{7}Li	3	p	3	−1.204	^{9}Be	5	^{8}Li	2_2	p	3	0.200
^{8}Be	0	^{7}Li	1	p	1	0.736	^{9}Be	7	^{8}Li	4	p	3	−0.323
^{8}Be	4	^{7}Li	3	p	3	−0.748	^{9}Be	7	^{8}Li	6	p	3	−0.899
^{8}Be	4	^{7}Li	3	p	1	−0.612	^{9}Be	7	^{8}Li	6	p	1	−0.564
^{8}Be	4	^{7}Li	1	p	3	0.667	^{7}Li	3	^{6}Li	2	n	3	0.657
^{8}Be	4	^{7}Li	7	p	3	0.624	^{7}Li	3	^{6}Li	2	n	1	−0.538
^{8}Be	4	^{7}Li	5_2	p	3	0.079	^{7}Li	3	^{6}Li	6	n	3	0.744
^{8}Be	4	^{7}Li	5_2	p	3	−0.146	^{7}Li	3	^{6}Li	4	n	3	−0.032
^{8}Be	8	^{7}Li	7	p	3	0.864	^{7}Li	3	^{6}Li	4	n	1	0.399
^{8}Be	8	^{7}Li	7	p	1	0.687	^{7}Li	1	^{6}Li	2	n	3	−0.925
^{8}Be	8	^{7}Li	5_2	p	3	0.374	^{7}Li	1	^{6}Li	2	n	1	0.197
^{8}Li	4	^{7}Li	3	n	3	−0.988	^{7}Li	1	^{6}Li	4	n	3	−0.555
^{8}Li	4	^{7}Li	3	n	1	0.237	^{7}Li	7	^{6}Li	6	n	3	−0.936
^{8}Li	4	^{7}Li	1	n	3	0.430	^{7}Li	7	^{6}Li	6	n	1	0.645
^{8}Li	4	^{7}Li	7	n	3	−0.496	^{7}Li	7	^{6}Li	4	n	3	−0.456
^{8}Li	4	^{7}Li	5	n	3	−0.665	^{7}Li	5_2	^{6}Li	2	n	3	−0.650
^{8}Li	4	^{7}Li	5_2	n	1	−0.275	^{7}Li	5_2	^{6}Li	6	n	3	0.732
^{8}Li	2_1	^{7}Li	3	n	3	0.567	^{7}Li	5_2	^{6}Li	6	n	1	0.549
^{8}Li	2_1	^{7}Li	3	n	1	0.351	^{7}Li	5_2	^{6}Li	4	n	3	0.200
^{8}Li	2_1	^{7}Li	1	n	3	0.905	^{7}Li	5_2	^{6}Li	4	n	1	−0.114
^{8}Li	2_1	^{7}Li	1	n	1	0.331	^{6}Li	2	d	2	α	0	0.907
^{8}Li	2_1	^{7}Li	5_2	n	3	0.767	^{6}Li	2	d	2	α	4	0.077
^{8}Li	6	^{7}Li	3	n	3	0.581	^{6}Li	6	d	2	α	4	0.943
^{8}Li	6	^{7}Li	5_2	n	3	−0.660	^{6}Li	6	d	2	α	8	0.028
^{8}Li	6	^{7}Li	5_2	n	1	−0.541	^{6}Li	4	d	2	α	4	0.929
^{8}Li	6	^{7}Li	7	n	3	0.973	^{9}Be	3	^{5}He	3	α	0	−0.925
^{8}Li	6	^{7}Li	7	n	1	−0.404	^{9}Be	3	^{5}He	3	α	4	0.784
^{8}Li	2_2	^{7}Li	3	n	3	−0.617	^{9}Be	5	^{5}He	3	α	4	0.974
^{8}Li	2_2	^{7}Li	3	n	1	−0.841	^{9}Be	5	^{5}He	3	α	8	−0.260
^{8}Li	2_2	^{7}Li	1	n	3	0.178	^{9}Be	7	^{5}He	3	α	4	0.882
^{8}Li	2_2	^{7}Li	1	n	1	0.331	^{9}Be	7	^{5}He	3	α	8	−0.737
^{8}Li	2_2	^{7}Li	5	n	3	0.231	^{7}Li	3	t	1	α	1	0.970
^{9}Be	3	^{8}Li	4	p	3	−0.947	^{7}Li	1	t	1	α	1	0.961
^{9}Be	3	^{8}Li	4	p	1	−0.319	^{7}Li	7	t	1	α	3	0.952
^{9}Be	3	^{8}Li	2_1	p	3	0.454	^{7}Li	5_2	t	1	α	3	0.223

the range of 40-60 degrees. It is interesting to note that we managed to describe within the CRC method the differential cross section of the ^{9}Be(d,p)^{10}Be^{gs} nuclear reaction in all scattering angles, including the range 40^0-60^0, where they were not covered in the Ref. [28, 19].

Sufficient contribution of the $3/2^- \to 2^+_1, 5/2^- \to 2^+_1, 7/2^- \to 2^+_1$ transitions was revealed for the p + ^{10}Be$^{3.37}$ channel in the entire range of scattering angles. In the cross section of the p + ^{10}Be$^{5.96}$ channel the theoretical calculation underestimates the experimental data starting from 70^0. Possibly, other higher excited states of ^{9}Be should be taken into account.

The Figure 8 illustrates the cross sections of the ^{9}Be(d,t)^{8}Be nuclear reaction at both 19.5 MeV and 35 MeV energies. As in the case of the (d,p) reactions, the (d,t) reactions also show the strong channel coupling effects. We see a manifestation of spin reorientation effects in the t+^{8}Be^{gs} channels and a valuable contribution of the $3/2^- \to 2^+, 5/2^- \to 2^+, 7/2^- \to 2^+$ transitions in the t+^{8}Be$^{3.03}$ channel.

Theoretical calculations made within the CRC method shows good agreement with experimental data for both (d,p) and (d,t) reactions. The analysis obtained strong coupling effects in both entrance and
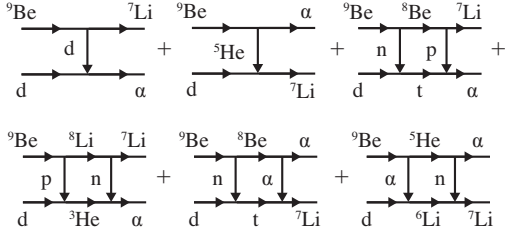
Figure 10. The scheme illustrates the reaction mechanisms taken into account in CRC calculations of the cross sections for ^{9}Be(d,α)^{7}Li reaction.

3.4. Cluster transfer reaction

Differential cross sections for the nuclear reaction ^{9}Be(d,α)^{7}Li are of particular interest. The reason is in specific behaviour of the cross section at large scattering angles, that shows possibility for the ^{5}He cluster transfer. In addition, the cross section calculated within the DWBA approach underestimates data even at forward scattering angles. Therefore, in order to cure the distinction between theory and experiment, the following transfer mechanisms are suggested (see Fig. 10):

– direct transfer of heavy clusters d and ^{5}He;

– sequential two-step transfer of n-p, p-n, n-α and α-n;

The resulting differential cross section for the ^{9}Be(d,α)^{7}Li reaction has form of a coherent sum of two amplitudes

$$\frac{d\sigma}{d\Omega}(\theta) = |f_I(\theta) + f_{II}(\theta)|^2, \tag{10}$$

where the amplitude

$$f_I(\theta) = f_{^5\mathrm{He}}(\pi - \theta) + f_{n-\alpha}(\pi - \theta) + f_{\alpha-n}(\pi - \theta) \tag{11}$$

describes the transfer of the heavy ^{5}He-cluster and sequential two-step transfer of n-α and α-n, and the amplitude

$$f_{II}(\theta) = f_d(\theta) + f_{n-p}(\theta) + f_{p-n}(\theta) \tag{12}$$

corresponds to the deuteron pick-up and sequential two-step transfer of n-p and p-n.

The DF potential (see Tab. 1) for the entrance channel and global optical potential parameterizations from Ref. [22, 29, 30] for intermediate and exit channels were used in the analysis. The prior form for the first coupling, and the post form for the second

exit channels. The effects of such kind were also emphasized in Ref. [18, 14].
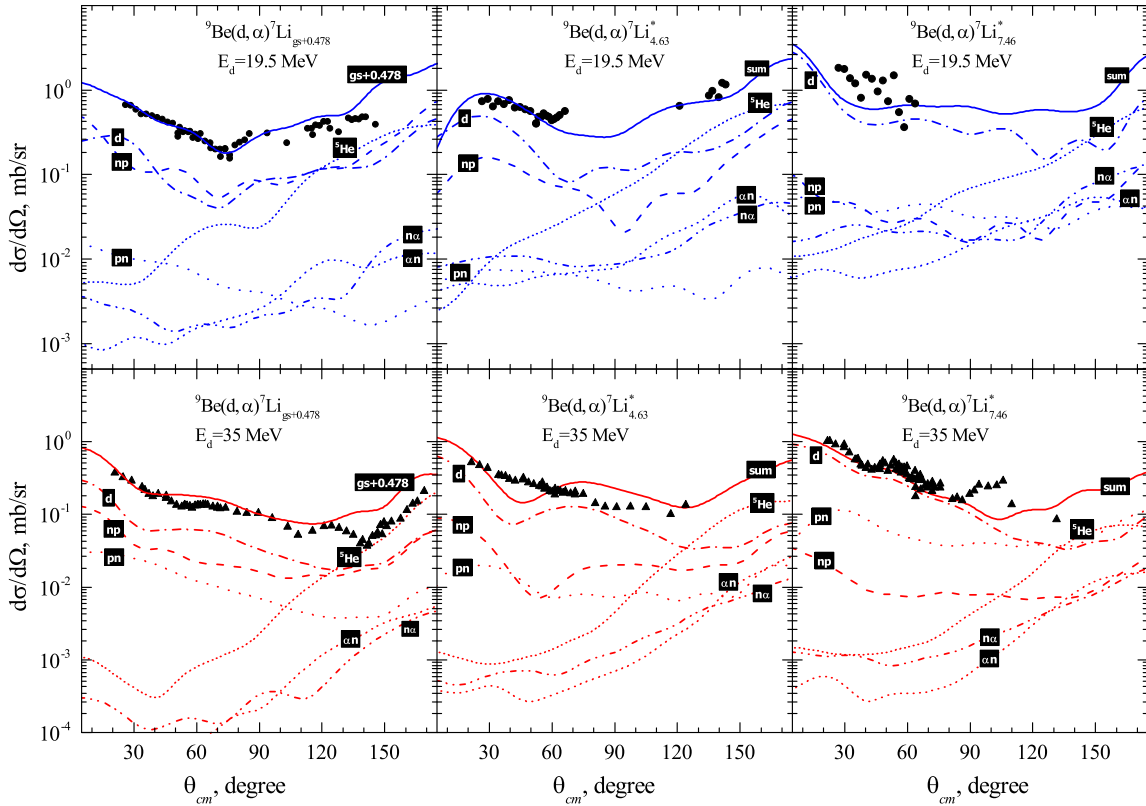
Figure 9. Differential cross sections for the ^{9}Be(d,α)^{7}Li reactions measured at 19.5 MeV and 35 MeV energy with the ^{7}Li observed in the ground or low-lying excited states in the exit channels.

coupling were chosen for two-step transfer reactions in order to avoid the non-orthogonal terms in the calculations of transition amplitudes.

The spectroscopic amplitudes of the d and ^{5}He clusters were taken from Ref. [31], while the alpha-cluster spectroscopic amplitudes given in Tab. 2 were provided by Dr. A. Volya within the method reported in Ref. [26].

The calculated cross sections are shown in Fig. 9 with the α-particle angular distributions formed in the ^{9}Be(d,α)^{7}Li* reaction at energies 19.5 and 35 MeV and corresponding to the low-lying excitation of the ^{7}Li nucleus in exit channels. The transfer of the deuteron (dash-dotted curve) provides the dominant contribution in all the channels. Despite the fact that the spectroscopic amplitude of the deuteron $\mathcal{S}_{1D_3} = 0.558$ in the ^{9}Be nucleus is not of great importance, a noticeable cross section is due to the large value of the deuteron spectroscopic amplitude $\mathcal{S}_{1S_1} = 1.732$ of ^{4}He.

The angular distribution of deuteron transfer has a significant cross section also at the back scattering angles, which is mainly caused by the contribution of the D wave. This symmetrical behaviour of the cross section of D waves is very similar to the cross section of evaporation residue. Tanaka et al. [32] analyzed the role of the compound process in ^{9}Be(d,α)^{7}Li reaction and claimed the domination of the compond nucleus channels at the 12.17 MeV and 14.43 MeV energies. However, in Ref. [19] the negligible contribution of mechanism through the compound nucleus was shown at 7 MeV using the DWBA analysis. In this regard, our theoretical results based on the CRC method shows that there is no need to take into account the mechanism through the compound nucleus at energies of 19.5 and 35.0 MeV.

In all channels starting from scattering angle $\theta_{c.m.} = 120°$ the transfer of the ^{5}He cluster, labeled as ^{5}He in Fig. 9, has a predominant contribution. It should be noted that the similiar result was mentioned early in Ref. [19]. One-step transfer of the ^{5}He cluster was also indicated as a dominant process by Jarczyk *et al* [33] studying the ^{12}C(^{11}B,^{6}Li)^{17}O and ^{12}C(d,^{7}Li)^{7}Be reactions.

Using the CRC method, we are able to estimate the contribution of the sequential transfer of the ^{5}He, which was not studied before. Corresponding cross sections are shown in Fig. 9 as curves labeled $n\alpha$ and αn. It turned out that the $n\alpha$ and the αn transfer processes provide indeed the contribution more than one order of magnitude lower in comparison with the one-step ^{5}He transfer. Nevertheless, it should be noted that the contribution of the n-α and the α-n transfer channels increases with the ^{7}Li excitation increases, where they should not be ignored.

The two-step n-p transfer is another mechanism
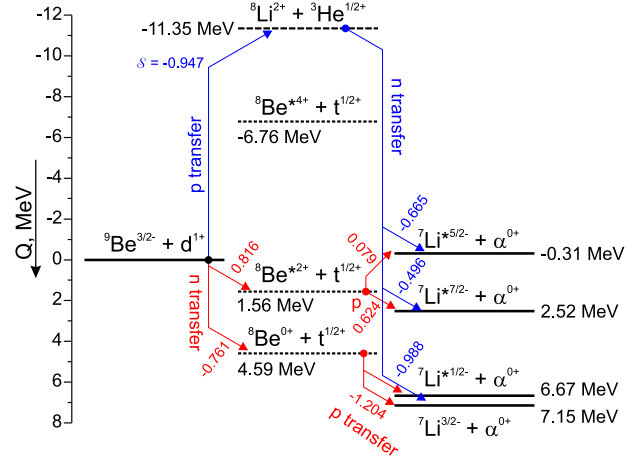
Figure 11. The scheme illustrates the energy balance of the different intermediate stages for the two-step mechanisms of ^{9}Be(d,α)^{7}Li transfer reaction. The Q-values for the different intermediate channels are shown near the corresponding lines. The numbers near the arrows correspond to the spectroscopic amplitudes of the heaviest reaction participants. For example, spectroscopic amplitude for the ^{9}Be = ^{8}Li + p configuration is equal $\mathcal{S} = -0.947$.

providing noticeable contribution to the cross section. It is due to the prominent cluster structure of the ^{9}Be nucleus having the weakly bound neutron. This structural feature explains also the weakness of the p-n sequential transfer contribution to the cross section corresponding the ^{7}Li(g.s.) in the exit channel. However curves in Fig. 11 with increasing the ^{7}Li excitation energy these two mechanisms change their places and the p-n transfer begins to play a leading role, providing, in particular, almost 10 times large contribution in the case of reaction at the $E_{lab} = 35$ MeV with ^{7}Li*(7.46 MeV) in exit channel.

In Fig. 11 the possible scenarios of the n-p and p-n sequential transferring for the reaction under consideration are shown in respect to the Q-values. One may see that all the steps of the n-p sequential transfer have the positive Q-values, while the p-n transfer goes through the intermediate channel ^{8}Li + ^{3}He having considerable negative Q-value. Together with large values of the spectroscopic amplitudes (shown near the arrows in Fig. 11) it explains the leading role of the (d,t;t,α) mechanism in populating the ground state of the ^{7}Li in the exit channel.

The situation becomes quite different in the case of the ^{7}Li*(5/2$^-$) in the exit channel. First of all the population of this state through the n-p transferring includes the ^{9}Be = ^{8}Be*(2$^+$) + n intermediate configuration where ^{8}Be cluster has to be in 2$^+$ excited state. Note that the ^{8}Be(0$^+$) ground state is inappropriate because of angular momentum coupling mismatch in entrance and exit configurations. Second circumstance is an extremely small spectroscopic
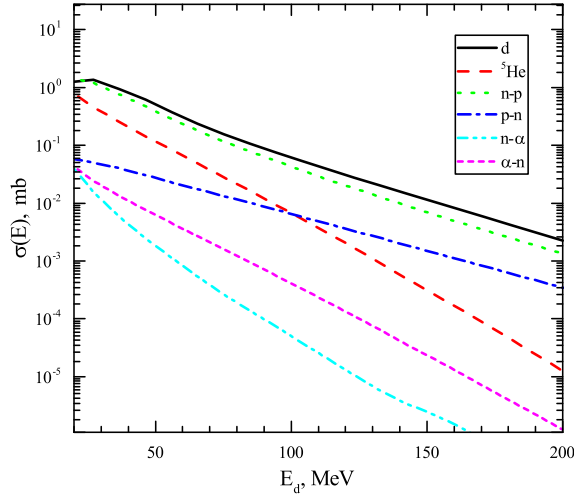
Figure 12. Contributions of the different mechanisms into the cross section of the ^{9}Be(d,α)^{7}Li$_{g.s.}$ reaction. See Fig. 10 for explanation of the curve notations.

amplitude of the ^{8}Be*(2$^+$) = ^{7}Li*(5/2$^-$) + p configuration which is equal $\mathcal{S}$ = 0.079. These two factors lead to the suppression of the contribution of (d,t;t,α) mechanism in population of the ^{7}Li*(5/2$^-$) state in the exit channel. Therefore the p-n sequential transfer prevails over the n-p one. With rising the collision energy the suppression of the (d,t;t,α) mechanism is even enhanced due to decrease the reaction time while the presence of the ^{8}Be*(2$^+$) intermediate state indicates that the process actually becomes multi-step one that requires more time.

Figure 12 shows the contributions of all the mechanism mentioned above into the total cross section of the ^{9}Be(d,α)^{7}Li$_{g.s.}$ reaction (see Fig. 10) as a function of the deuteron energy. One may conclude that only four mechanisms form the cross section of this reaction mainly. The transfer of the deuteron-cluster is predominant channel at the all collision energies. The sequential n-p and p-n transfers play significant role at the high energies. The ^{5}He-cluster transfer gives almost 20% of the cross section at low energies and outgoes the sequential p-n transfer in this energy domain. Thus it allows us to claim that the configurations $n+^8$Be and $\alpha + ^5$He provide noticeable contributions into the ground state wave function of the ^{9}Be nucleus. These conclusions agree well with the previous experimental studies [8, 9].

4. Conclusion

In the present work, the deuteron induced reactions with ^{9}Be target have been studied at the collision energies 19.5 and 35 MeV. The calculated double folding potential has been applied successfully in the describing of crsoss sections of elastic and inelastic scatterings, one nucleon transfer and cluster transfer reactions. The deformation parameter of transition $3/2^- \rightarrow 5/2^-$ of ^{9}Be has been obtained. The strong coupling effects have been shown on the example of the (d,p) and (d,t) one nucleon transfer nuclear reactions. It was found that in the ^{9}Be(d,α)^{7}Li nuclear reaction the ^{5}He heavy cluster is transferred mainly simultaneously, and the contribution of its sequential transfer is an order of magnitude lower. The importance of taking into account the mechanism of sequential transfer of the n-p system has been revealed. Based on these it can be concluded that studying the interaction of the deuteron with ^{9}Be the ^{9}Be nucleus has cluster structure.

Acknowledgments

References

[1] Wang M, Audi G, Wapstra A H, Kondev F G, MacCormick M, Xu X and Pfeiffer B 2012 *Chin.Phys.C* **36** 1603
[2] Sundholm D and Olsen J 1991 *Chem.Phys.Lett.* **177** 91
[3] Kukulin V I and Voronchev V T 2010 *Phys.Atomic Nuclei* **73** 1376
[4] Seksembayev Z, Kukulin V and Sakhiyev S 2018 *Physica Scripta* **93** 085602
[5] Lukyanov S M, Denikin A S, Voskoboynik E I, Khlebnikov S V, Harakeh M N, Maslov V A, Penionzhkevich Y E, Sobolev Y G, Trzaska W H, Tyurin G P and Kuterbekov K A 2014 *J.Phys.(London)* **G41** 035102
[6] Lukyanov S M, Harakeh M N, Naumenko M A, Xu Y, Trzaska W H, Burjan V, Kroha V, Mrazek J, Glagolev V, Piskor S, Voskoboynik E I, Khlebnikov S V, Penionzhkevich Y E, Skobelev N K, Sobolev Y G, Tyurin G P, Kuterbekov K and Tuleushev Y 2015 *World Journal of Nuclear Science and Technology* **5** 265
[7] Janseitov D M, Lukyanov S M, Mendibayev K, Penionzhkevich Y E, Skobelev N K, Sobolev Y G, Kuterbekov K A, Valiolda D S, Zholdybayev T K, Trzaska W H, Khlebnikov S V, Tyurin G P, Urazbekov B A, Harakeh M N, Burjan V, Kroha V, Mrazek J, Piskor S, Sivacek I and Glagolev V 2018 *Int.J.Mod.Phys.* **E27** 1850089
[8] Brown T A D, Papka P, Fulton B R, Watson D L, Fox S P, Groombridge D, Freer M, Clarke N M, Ashwood N I, Curtis N, Ziman V, McEwan P, Ahmed S, Catford W N, Mahboub D, Timis C N, Baldwin T D and Weisser D C 2007 *Phys.Rev. C* **76** 054605
[9] Papka P, Brown T A D, Fulton B R, Watson D L, Fox S P, Groombridge D, Freer M, Clarke N M, Ashwood N I, Curtis N, Ziman V, McEwan P, Ahmed S, Catford W N, Mahboub D, Timis C N, Baldwin T D and Weisser D C 2007 *Phys.Rev. C* **75** 045803
[10] Detraz C, Duhm H H and Hafner H 1970 *Nucl.Phys.* **A147** 488

[11] Detraz C, Pougheon F, Bernas M, Langevin M, Roussel P and Vernotte J 1974 *Nucl.Phys.* **A228** 39

[12] Urazbekov B A, Denikin A S, Sakhiev S K and Burtebaev N T 2016 *Bull.Rus.Acad.Sci.Phys.* **80** 247

[13] Urazbekov B A, Denikin A S, Sakhiev S K and Lukyanov S M 2017 *Bull.Rus.Acad.Sci.Phys.* **81** 690

[14] Rudchik A T, Chercas K A, Kemper K W, Rusek K, Rudchik A A, Herashchenko O V, Koshchy E I, Pirnak V M, Piasecki E, Trzcinska A, Sakuta S B, Siudak R, Strojek I, Stolarz A, Ilyin A P, Ponkratenko O A, Stepanenko Y M, Shyrma Y O, Szczurek A and Uleshchenko V V 2016 *Nucl.Phys.* **A947** 161

[15] Thompson I J 1988 *Computer Physics Reports* **7** 167 – 212

[16] Kunz P D Computer code DWUCK5 unpublished

[17] Karpov A, Denikin A, Naumenko M, Alekseev A, Rachkov V, Samarin V, Saiko V and Zagrebaev V 2017 *Nuclear Instruments and Methods in Physics Research Section A: Accelerators, Spectrometers, Detectors and Associated Equipment* **859** 112 – 124

[18] Harakeh M N, Van Popta J, Saha A and Siemssen R H 1980 *Nucl.Phys.* **A344** 15

[19] Szczurek A, Bodek K, Krug J, Lubcke W, Ruhl H, Steinke M, Stephan M, Kamke D, Hajdas W, Jarczyk L, Kamys B, Strzalkowski A and Kwasniewicz E 1989 *Z.Phys.* **A333** 271

[20] Votava H J, Clegg T B, Ludwig E J and Thompson W J 1973 *Nucl.Phys.* **A204** 529

[21] Koning A J and Delaroche J P 2003 *Nucl.Phys.* **A713** 231

[22] Li X, Liang C and Cai C 2007 *Nucl.Phys.* **A789** 103

[23] Caurier E, Martínez-Pinedo G, Nowacki F, Poves A and Zuker A P 2005 *Rev. Mod. Phys.* **77**(2) 427–488

[24] Cohen S and Kurath D 1965 *Nucl.Phys.* **73** 1

[25] Volya A *Private communication. Unpublished*

[26] Kravvaris K and Volya A 2017 *Phys.Rev.Lett.* **119** 062501

[27] Della Rocca V and Iachello F 2018 *Nucl.Phys.* **A973** 1

[28] Galanina L I and Zelenskaya N S 2012 *Physics of Part.and Nuclei* **43** 147

[29] Avrigeanu V, Hodgson P E and Avrigeanu M 1994 *Phys.Rev.* **C49** 2136

[30] Cook J 1982 *Nucl.Phys.* **A388** 153

[31] Kwasniewicz E and Jarczyk L 1985 *Nucl.Phys.* **A441** 77

[32] Tanaka S 1978 *J.Phys.Soc.Jpn.* **44** 1405

[33] Jarczyk L, Kamys B, Kistryn M, Magiera A, Rudy Z, Strzalkowski A, Barna R, D'Amico V, De Pasquale D, Italiano A and Licandro M 1996 *Phys.Rev.* **C54** 1302

[34] CANAM URL http://canam.ujf.cas.cz/